

Title:	A Modular Multilevel Matrix Converter for High Speed Drive Applications
Authors:	Dennis Bräckle, Felix Kammerer, Mathias Schnarrenberger, Marc Hiller, Michael Braun
Institute:	Karlsruhe Institute of Technology (KIT) Elektrotechnisches Institut (ETI)
Type:	Conference Proceedings
Published at:	Proceedings 2016 PCIM Europe, International Conference and Exhibition for Power Electronics, Intelligent Motion, Renewable Energy and Energy Management, Nuremberg, Germany, May 10-12, 2016 Publisher: VDE Verlag Year: 2016 ISBN: 978-3-8007-4186-1 Pages: 788 - 795
Hyperlinks:	<a href="http://www.pcim-europe.com">http://www.pcim-europe.com</a>

# A Modular Multilevel Matrix Converter for High Speed Drive Applications

Dennis Bräckle, Felix Kammerer, Mathias Schnarrenberger, Marc Hiller, Michael Braun  
 Elektrotechnisches Institut (ETI) - Power Electronic Systems  
 Karlsruhe Institute of Technology (KIT), Kaiserstraße 12, 76131 Karlsruhe, Germany  
 Fon: +49 721 608 42922, E-Mail: dennis.braeckle@kit.edu

## Abstract

The Modular Multilevel Matrix Converter (M3C) performs a direct three-phase AC to AC power conversion and is highly suitable for medium voltage high power drive applications. One area of application are high speed drives such as compressors. However, additional balancing power components which reduce the output power capability of the M3C when input and output frequencies are similar occur. This paper analytically examines the operation behavior and power capability in these operation points in order to assess whether the M3C can generate these additional components without oversizing the converter's components. Subsequently, the theoretical evaluation is verified by a laboratory scaled prototype with a rated power of 15 kW.

## 1. Fundamentals of the M3C topology

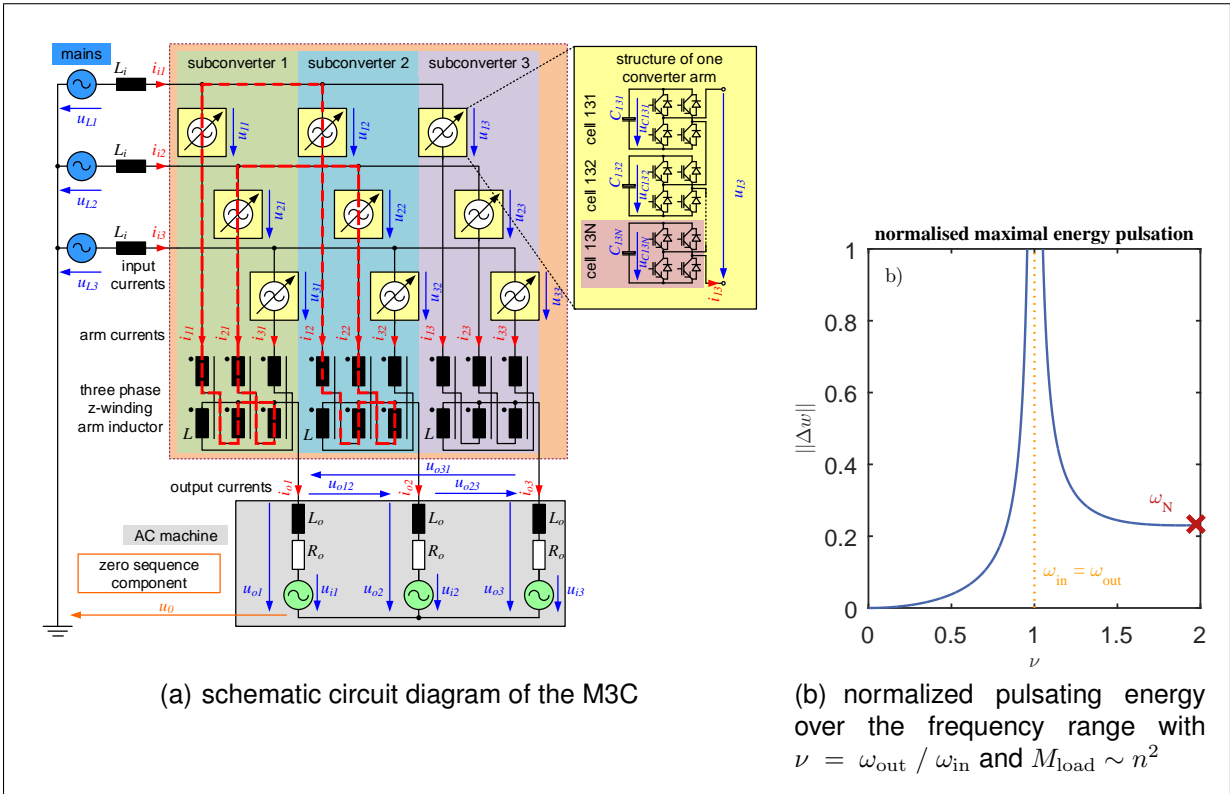


Fig. 1

Figure 1 a) shows the schematic structure of the overall system with the AC-grid, the Modular Multilevel Matrix Converter (M3C) and an AC machine. The M3C is composed of 3 subcon-

verters. Each subconverter connects the three input phases to one of the output phases, using converter arms and arm inductances  $L$ . The converters consist of  $N$  series connected cells in H-bridge configuration. Each cell has a capacitor  $C_{xyz}$  ( $x$ : input phase,  $y$ : output phase,  $z$ : cell number) and is able to generate a voltage of  $-\sum_{z=1}^N u_{Cxyz} \leq u_{xy} \leq \sum_{z=1}^N u_{Cxyz}$ . The M3C has been proven suitable for low frequency high torque drive applications [1] and for high speed drive applications [2]. Figure 1 (b) shows the normalized total energy pulsations  $\|\Delta w\|$  over the positive frequency range when driving a machine with  $\omega_N = 2\omega_i$  and a quadratic load characteristic. The converter's components are designed for the nominal operation point of the driven machine. The maximum energy pulsation at  $\omega_o \approx \omega_i$  is a criterion for dimensioning the cell capacitors. However, when  $\omega_o \approx \omega_i$ , additional low frequent power components occur. They have to be compensated in order to reduce the total  $\Delta w$ . Using the control strategies presented in [3] and [4], additional balancing currents and a zero sequence voltage are generated to ensure stable operation at  $\omega_o \approx \omega_i$ . The maximum current in each arm is limited by semiconductors and designed for the nominal operation point of the machine. In order to determine the available performance at  $\omega_o \approx \omega_i$ , the maximum balancing power and current limits are calculated and verified with a laboratory scaled prototype with a rated power of  $P = 15\text{kW}$  and  $N = 5$  cells per converter arm.

## 2. Fundamentals of the M3C control strategy

The M3C is a highly complex topology with several degrees of freedom that need to be considered adequately when implementing a control scheme. First, the 9 arm currents need to be controlled in order to drive the load machine and exchange power with the feeding grid. There are 8 degrees of freedom and the constraint  $\sum i_{xy} = 0$ . Secondly, the converter's energy must be distributed equally among all capacitors. The control scheme presented in [3] separates the modulation of each arm from the converter control. The equivalent circuit diagram is shown in Figure 1(a). With this analysis, the important power components are identified and examined when driving a high speed machine.

### 2.1. Arm converter power control

In [3] a new control scheme based on a transformed arm power analysis is presented. The measured currents and capacitor voltages can be transformed so that a decoupled control of the input side, the output side and two inner components is possible. The power for each arm can be calculated with the arm voltage and arm current  $p_{xy} = u_{xy} \cdot i_{xy}$ . For converter arm 11 the resulting power component is

$$p_{11} = u_{11} \cdot i_{11} \approx (u_{i,\alpha} - u_{o,\alpha} - u_0) \cdot \left( \frac{i_{i,\alpha}}{3} + \frac{i_{o,\alpha}}{3} + i_{d1,\alpha} + i_{d2,\alpha} \right) \quad (1)$$

The resulting arm power consists of the  $\alpha$ -components of the input voltage  $u_i$ , the output voltage  $u_o$  and the zero sequence voltage  $u_0$  multiplied by the sum of the  $\alpha$ -components of the input current  $\frac{i_i}{3}$ , the output current  $\frac{i_o}{3}$  and the internal currents  $i_{d1}$  and  $i_{d2}$ . The calculated arm powers are also transformed with respect to the rules in [3]. Due to the different frequencies occurring in the power components, some must be considered separately during operation with similar input and output frequencies (see section 2.2).

## 2.2. Operational management when feeding a high frequency drive

The M3C performs a direct 3AC-3AC energy conversion. It is suitable for driving machines whose nominal frequency is larger than the input frequency [2]. When running up the machine, the point of similar input and output frequency has to be overcome. At that point the frequency of inner reactive power components become low frequent and cause a large energy fluctuation in the cell capacitors. These components have to be compensated in order to assure stable operation of the M3C. According to the transformation in [3] and assuming sinusoidal functions with  $\gamma = \omega t$  for all current and voltage components the resulting inner power components  $p_{d1,\alpha\beta}$  and  $p_{d2,\alpha\beta}$  are

$$p_{d1\alpha} = \frac{1}{2}\hat{U}_i\hat{I}_{d2}\cos(\gamma_i + \gamma_{d2}) - \frac{1}{2}\hat{U}_o\hat{I}_{d2}\cos(\gamma_o + \gamma_{d2}) + \frac{1}{2}\hat{U}_0\hat{I}_{d1}\cos(\gamma_0 \pm \gamma_{d1}) + \frac{1}{6}\hat{U}_i\hat{I}_o\cos(-\gamma_i + \gamma_o + \varphi_o) - \frac{1}{6}\hat{U}_o\hat{I}_i\cos(\gamma_o - \gamma_i - \varphi_i) \quad (2)$$

$$p_{d1\beta} = \frac{1}{2}\hat{U}_i\hat{I}_{d2}\sin(\gamma_i + \gamma_{d2}) - \frac{1}{2}\hat{U}_o\hat{I}_{d2}\sin(\gamma_o + \gamma_{d2}) + \frac{1}{2}\hat{U}_0\hat{I}_{d1}\sin(\gamma_0 \pm \gamma_{d1}) + \frac{1}{6}\hat{U}_i\hat{I}_o\sin(-\gamma_i + \gamma_o + \varphi_o) - \frac{1}{6}\hat{U}_o\hat{I}_i\sin(\gamma_o - \gamma_i - \varphi_i) \quad (3)$$

$$p_{d2\alpha} = \frac{1}{2}\hat{U}_i\hat{I}_{d1}\cos(-\gamma_i + \gamma_{d1}) - \frac{1}{2}\hat{U}_o\hat{I}_{d1}\cos(\gamma_o + \gamma_{d1}) + \frac{1}{2}\hat{U}_0\hat{I}_{d2}\cos(\gamma_0 \pm \gamma_{d2}) + \frac{1}{6}\hat{U}_i\hat{I}_o\cos(\gamma_i + \gamma_o + \varphi_o) - \frac{1}{6}\hat{U}_o\hat{I}_i\cos(\gamma_o + \gamma_i - \varphi_i) \quad (4)$$

$$p_{d2\beta} = \frac{1}{2}\hat{U}_i\hat{I}_{d1}\sin(-\gamma_i + \gamma_{d1}) - \frac{1}{2}\hat{U}_o\hat{I}_{d1}\sin(\gamma_o + \gamma_{d1}) + \frac{1}{2}\hat{U}_0\hat{I}_{d2}\sin(\gamma_0 \pm \gamma_{d2}) + \frac{1}{6}\hat{U}_i\hat{I}_o\sin(\gamma_i + \gamma_o + \varphi_o) - \frac{1}{6}\hat{U}_o\hat{I}_i\sin(\gamma_o + \gamma_i - \varphi_i) \quad (5)$$

The second line in each of the equations (2)-(5) is defined by the feeding grid and load machine. The power components depend on the input voltage  $\hat{U}_i$ , current  $\hat{I}_i$  and phase shift  $\varphi_i$  as well as the output voltage  $\hat{U}_o$ , current  $\hat{I}_o$  and phase shift  $\varphi_o$ . These components become low frequent and cause energy fluctuations during operation with  $\omega_i \approx \omega_o$ . Therefore, they have to be compensated. Otherwise stable operation of the M3C can not be guaranteed. The first line of the equations can be controlled separately. Using the internal currents  $\hat{I}_{d1}$  and  $\hat{I}_{d2}$  and the zero sequence voltage  $\hat{U}_0$ , these components compensate the low frequent reactive power (see section 3.2) and assure stable operation of the M3C.

## 3. Operation points with similar input and output frequencies

### 3.1. Compensation of power components

As discussed in 2.2, low frequent reactive power components occur during operation with similar input and output frequencies. An analytical discussion for compensating these components is presented. The following discussion is only focusing on inner power component 1  $p_{d1,\alpha\beta}$  (eq. (2) and (3)) with corresponding results to component 2  $p_{d2,\alpha\beta}$ . The occurring low frequent

components are

$$\begin{aligned}
p_{d1,lf,\alpha} &= \frac{1}{6} \hat{U}_i \hat{I}_o \cos(-\gamma_i + \gamma_o + \varphi_o) - \frac{1}{6} \hat{U}_o \hat{I}_i \cos(\gamma_o - \gamma_i - \varphi_i) \\
p_{d1,lf,\beta} &= \frac{1}{6} \hat{U}_i \hat{I}_o \sin(-\gamma_i + \gamma_o + \varphi_o) - \frac{1}{6} \hat{U}_o \hat{I}_i \sin(\gamma_o - \gamma_i - \varphi_i) \\
\hat{p}_{d1,lf} &= \sqrt{p_{d1,lf,\alpha}^2 + p_{d1,lf,\beta}^2} \\
&= \frac{1}{6} \cdot \sqrt{(\hat{U}_i \hat{I}_o)^2 + (\hat{U}_o \hat{I}_i)^2 - 2 \hat{U}_i \hat{I}_o \hat{U}_o \hat{I}_i \cdot \cos(\varphi_i + \varphi_o)}
\end{aligned} \tag{6}$$

Several assumptions are made:

- losses are neglected
- the ratio between input voltage  $\hat{U}_i$  and output voltage  $\hat{U}_o$  is  $k_u$
- the ratio between the output power  $S_o$  and the nominal output power  $S_{o,N} = \frac{1}{6} \hat{U}_{o,N} \hat{I}_{o,N}$  is  $s$
- the worst-case-scenario of the maixmal balancing power is considered

With these assumptions the input current can be written as

$$\begin{aligned}
P_{in} &= P_{out} \\
\frac{\sqrt{3}}{2} \hat{U}_i \hat{I}_i \cos(\varphi_i) &= \frac{\sqrt{3}}{2} \hat{U}_o \hat{I}_o \cos(\varphi_o) \\
\hat{I}_i &= \hat{I}_o k_u \frac{\cos(\varphi_o)}{\cos(\varphi_i)}
\end{aligned} \tag{7}$$

Combining equation (6) and (7), the resulting, normalized power component  $p_{bal}$  needing to be compensated is

$$\begin{aligned}
p_{bal} &= \frac{\hat{p}_{d1,lf}}{S_{o,N}} = \frac{\frac{1}{6} (\hat{U}_o \hat{I}_o)}{\frac{1}{6} (\hat{U}_{o,N} \hat{I}_{o,N})} \cdot \sqrt{\frac{1}{k_u^2} + \frac{k_u^2 \cos^2(\varphi_o)}{\cos^2(\varphi_i)} - 2 \frac{\cos(\varphi_o)}{\cos(\varphi_i)} \cos(\varphi_o + \varphi_i)} \\
p_{bal} &= \frac{s}{\cos(\varphi_i)} \cdot \sqrt{\frac{\cos^2(\varphi_i)}{k_u^2} + k_u^2 \cos^2(\varphi_o) - 2 \cos(\varphi_i) \cos(\varphi_o) \cos(\varphi_i + \varphi_o)}
\end{aligned} \tag{8}$$

Equation (8) shows the power component that has to be compensated in order to overcome the point of similar input and output frequency to accelerate a load machine to nominal frequencies beyond the input frequency. According to equation (2) to (5) the superposition of the low frequent components results in a sinusoidal reactive power component with an amplitude  $p_{bal}$  and a frequency  $\omega_{bal}$ , which is not considered because of the worst-case consideration.  $p_{bal}$  provides information whether the pulsating power components can be compensated without oversizing the converter. In addition, the generation of the balancing power must be considered with respect to the current and voltage capability of the converter (see section 3.2).

### 3.2. Generation of the balancing power components

[3] and [5, 4] show control techniques that allow the compensation of the balancing power  $p_{bal}$  from equation (8). In [3] the balancing power is generated with an balancing current  $i_{bal,[3]}$  and a zero sequence voltage  $u_0$ . The zero sequence voltage is a degree of freedom when the neutral

points of the input and output side are not connected and a common mode voltage is allowed on both sides. [4] presents a method where the power is generated with an internal current  $i_{\text{bal},[4]}$  and the output voltage  $u_o$ . The arm currents of the M3C are composed of  $i_{\text{arm}} = \frac{i_i}{3} + \frac{i_o}{3} + i_{\text{bal}}$ . The semiconductors of the converter arms are designed for nominal operation of the machine. Neglecting losses, the maximum arm current is  $i_{\text{arm,max}} = \frac{i_{i,N}}{3} + \frac{i_{o,N}}{3}$ . Normalised on the nominal output power, the maximum amplitude of the arm current is given by  $|\hat{I}_{\text{arm,max}}| = 0.67$ . With both proposed controlling methods, the balancing power from equation (8) can be generated. Depending on the operational conditions, either method [3] or [4] may be used. The resulting rated balancing current amplitudes are

$$i_{\text{bal},[3]} = \sqrt{\frac{1}{36} \cdot \frac{S_o^2 k_u \cos^2(\varphi_o)}{\cos^2(\varphi_i) u_0^2} + \frac{1}{36} \cdot \frac{S_o^2}{k_u^2 u_0^2} - \frac{1}{18} \cdot \frac{S_o^2 \cos(\varphi_o) \cos(\varphi_o - \varphi_i)}{\cos(\varphi_i) u_0^2}} \quad (9)$$

$$i_{\text{bal},[4]} = \frac{1}{3} \cdot \sqrt{\frac{i_o^2 k_u^2 \cos^2(\varphi_o)}{\cos^2(\varphi_i)} + i_o^2} \quad (10)$$

The balancing current is an additional current that reduces the output current capability when driving a load with similar input and output frequency. A converter, designed for nominal operation of a high speed drive, is able to accelerate this machine without oversizing the semiconductors if the maximum arm current is not exceeded during operation with similar input and output frequencies.

#### 4. Experimental setup and final results

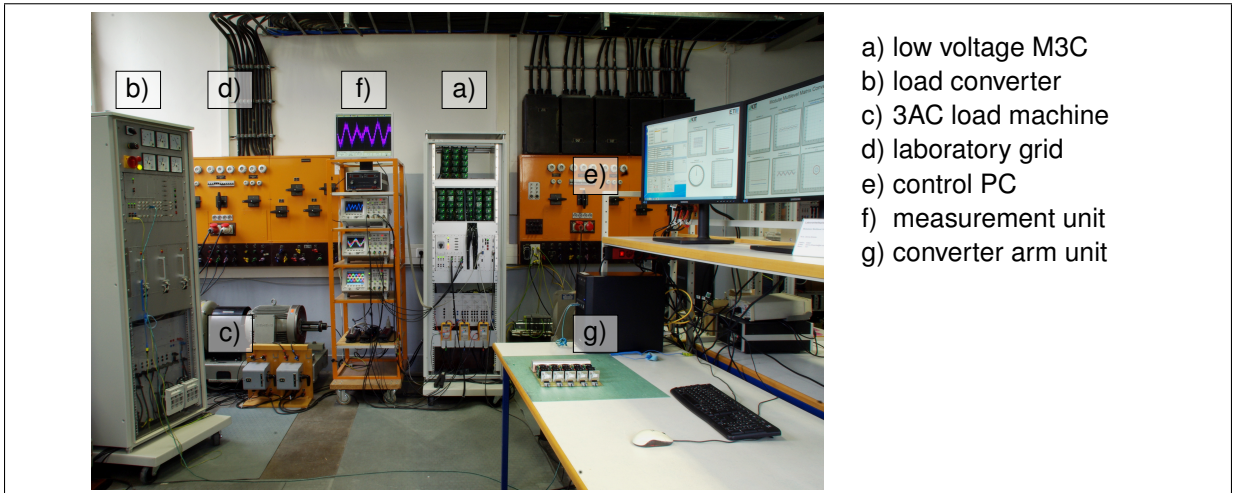


Fig. 2: low voltage laboratory prototype of the M3C with  $P_N = 15\text{kW}$ , signal processing unit and load machine/resistive load

Figure 2 (a) shows the laboratory setup for measurement and verification of the theoretical discussion. The low voltage prototype has a rated power of  $P_N = 15\text{kW}$ . It consists of  $N = 9 \cdot 5 = 45$  cells with a local microcontroller (dsPIC from Microchip) in each cell. They are connected via optical fiber to a FPGA (Altera) as central modulation unit. The control scheme presented in [3, 6, 7] is programmed on a TMS320C6748 digital signal processor unit from Texas Instruments. The period of the control algorithm is  $T_{\text{ctrl}} = T_{\text{PWM}} = \frac{1}{f_{\text{PWM}}} = 125\mu\text{s}$ . The prototype can feed an AC-machine (depicted in figure 2) or a resistive load. The prototype

operates over the whole frequency range[3] and is used to verify the results presented in this paper.

#### 4.1. Experimental results of the balancing power analysis

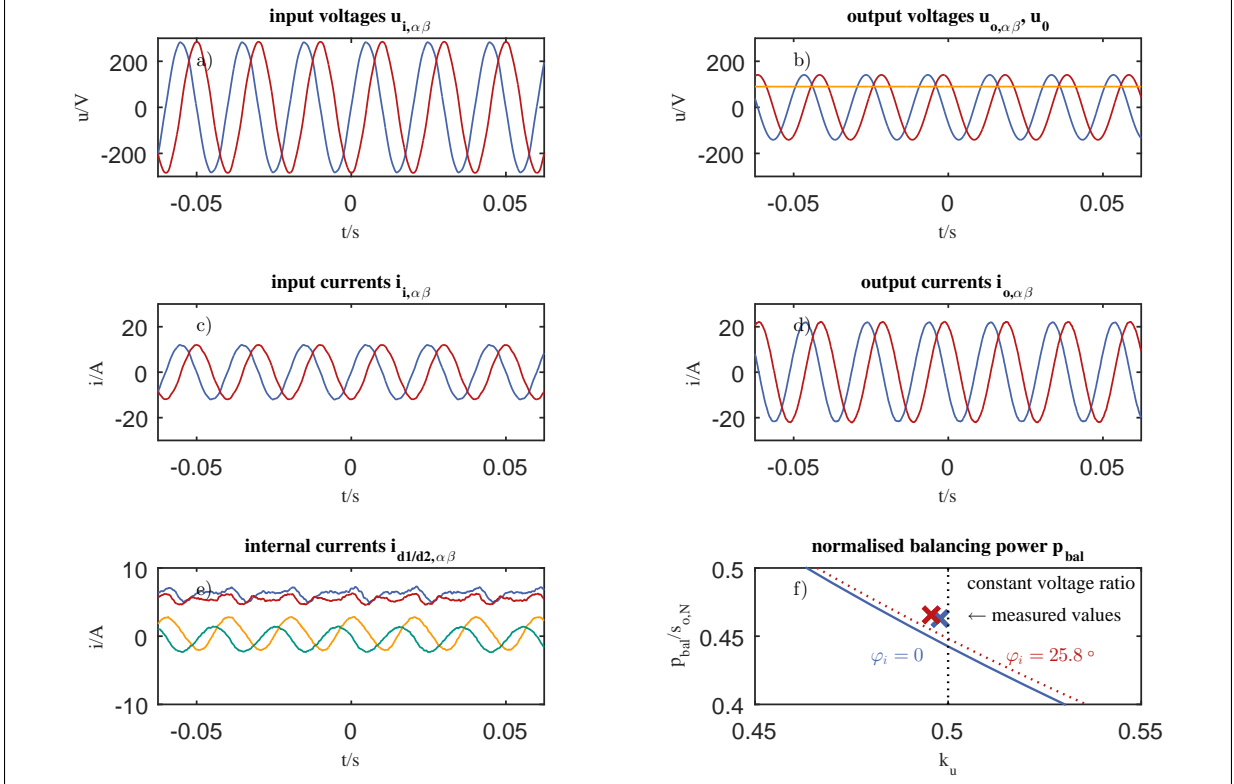


Fig. 3: a)-e) measurements of the laboratory prototype with a passive load at  $\omega_o = 50\text{Hz}$ ,  $s \approx 0.29$ ,  $\varphi_i = 0$  and  $k_u \approx 0.5$ , short time averaged values at  $T_A = \frac{1}{f_{PWM}} = \frac{1}{8\text{kHz}}$ , f) compares the calculated and actual balancing power components at different  $\varphi_i = 0$

Figure 3 shows experimental results from a laboratory prototype of the M3C [1] to verify the results from equation (8). The phase shift on the output side  $\varphi_o$  is defined by the load. The phase shift on the input side  $\varphi_i$  is a degree of freedom. In order to generate the balancing power, additional voltages and internal currents are necessary. The sum of the normalised output power  $s_o$  and balancing power  $p_{bal}$  must not exceed 1 to avoid an oversizing of the converter components. Figure 3 a)-d) depict the measured input and output values of the M3C laboratory prototype at  $\omega_o = 50\text{Hz}$  and a passive load. The output phase shift is  $\varphi_o = 0$ . The output power is  $P_o = 0.29 \cdot P_{o,N} = 4.35\text{kW}$ . Figure 3 e) shows the internal balancing currents. The additional balancing power is generated with the DC zero sequence voltage  $u_0$  and the internal balancing currents. Figure 3 f) compares the theoretical balancing power  $p_{bal}$  in equation (8) and the measured power. Additionally, the effect of different phase shifts  $\varphi_i$  on the input side are examined.

The M3C is a symmetric system. Reactive power, either on the input or the output side, results in an additional balancing power when  $\omega_i \approx \omega_o$ . The discrepancy between the theoretical and measured balancing power in Figure 3 f) is only approx. 4% and results from the assumption of ideal conditions, e.g. neglecting losses. The results therefore verify the analytical discussion of the balancing power.

## 4.2. Maximum output current capability with additional balancing current

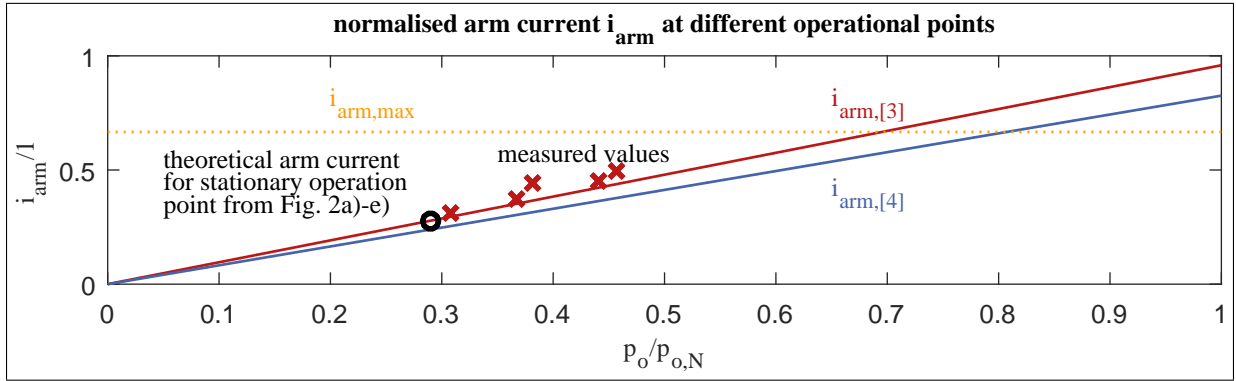


Fig. 4: normalised arm currents ( $i_{arm} = \frac{i_i}{3} + \frac{i_o}{3} + i_{bal}$ ) according to [3] and [4] at constant output voltage ratio  $k_u \approx 0.5$  and different output powers.

Figure 4 depicts the normalized arm currents  $i_{arm} = \frac{i_i}{3} + \frac{i_o}{3} + i_{bal}$ . The output voltage ratio is constant  $k_u \approx 0.5$ . Assuming a quadratic load characteristic, the maximum arm current  $|\hat{i}_{arm,max}|$  (dashed yellow line) is not reached. Therefore the remaining arm current capability can be used to generate additional output current when operating at similar input and output frequencies. Transferred to a drive application, the additional current can generate an acceleration torque e.g. for accelerating the AC machine to its nominal speed without oversizing the semiconductors. Measurements with different output currents verify that additional output power can be provided.

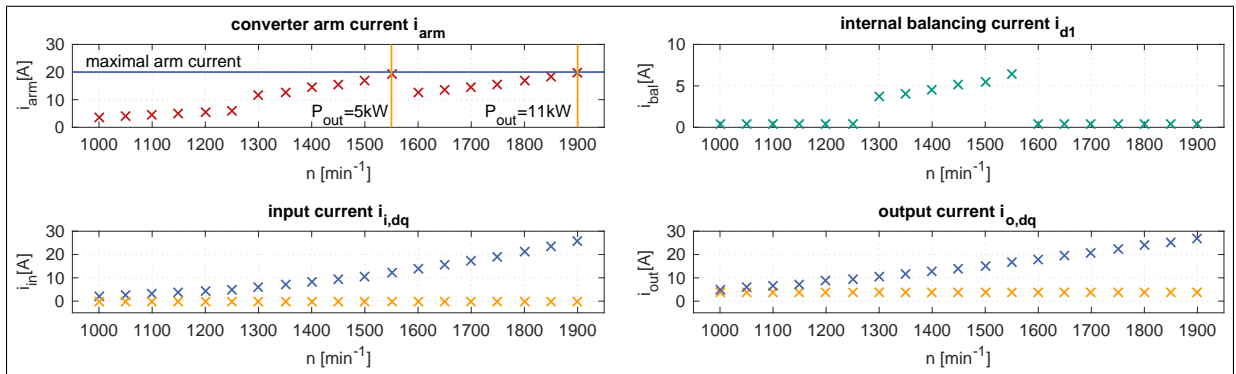


Fig. 5: short time averaged measurements with the prototype when driving a machine and a quadratic load profile. In addition the balancing, input and output currents

In Figure 5, an acceleration of an induction machine from  $n_0 = 1000\text{min}^{-1}$  to  $n_1 = 1900\text{min}^{-1}$  is shown. The load is a converter-fed DC machine with a quadratic load profile. During acceleration, the point of similar input and output frequency must be overcome. Therefore, additional internal currents are produced to compensate the power components from equation (8). The maximum arm current is never exceeded. It reaches its maximum value ( $i_{arm,max} = 20A$ ) where the output frequency is similar to the input frequency and where  $n_{IM} = n_1$ . The machine can be accelerated without oversizing the converters semiconductors.

## 5. Conclusion

This paper presents an analytical solution for the performance of the Modular Multilevel Matrix Converter (M3C) in operation points for similar input and output frequencies. The necessary balancing power and the effect on the limit of the arm currents are calculated. A laboratory scaled prototype with a rated power of 15 kW demonstrates the outstanding performance of the M3C. With this results, the M3C is suitable for high speed drive applications where  $\omega_N = 2\omega_i$  and a quadratic load characteristic. The current limits allow additional output currents to accelerate a load machine to its nominal speed. Subsequently, the cell capacitors and semiconductors of the M3C do not have to be oversized in order to accelerate a machine with a high nominal frequency e.g. for compressor applications.

## 6. Acknowledgment

The authors would like to thank the DFG (German Research Foundation) which finances this research project under grant BR 1780/8-2.

## 7. References

- [1] F. Kammerer, D. Braeckle, M. Gommeringer, M. Schnarrenberger, and M. Braun. Operating performance of the modular multilevel matrix converter in drive applications. In *PCIM Europe 2015; International Exhibition and Conference for Power Electronics, Intelligent Motion, Renewable Energy and Energy Management; Proceedings of*, pages 1–8, 2015.
- [2] K. Ilves, L. Bessegato, and S. Norrga. Comparison of cascaded multilevel converter topologies for ac/ac conversion. In *Power Electronics Conference (IPEC-Hiroshima 2014 - ECCE-ASIA), 2014 International*, pages 1087–1094, 2014.
- [3] F. Kammerer, M. Gommeringer, J. Kolb, and M. Braun. Energy balancing of the modular multilevel matrix converter based on a new transformed arm power analysis. In *Power Electronics and Applications (EPE'14-ECCE Europe), 2014 16th European Conference on*, pages 1–10, 2014.
- [4] W. Kawamura, M. Hagiwara, and H. Akagi. A broad range of frequency control for the modular multilevel cascade converter based on triple-star bridge-cells (mmcc-tsbc). In *Energy Conversion Congress and Exposition (ECCE), 2013 IEEE*, pages 4014–4021, 2013.
- [5] W. Kawamura, M. Hagiwara, and H. Akagi. Control and experiment of a 380-v, 15-kw motor drive using modular multilevel cascade converter based on triple-star bridge cells (mmcc-tsbc). In *Power Electronics Conference (IPEC-Hiroshima 2014 - ECCE-ASIA), 2014 International*, pages 3742–3749, May 2014.
- [6] F. Kammerer, J. Kolb, and M. Braun. Fully decoupled current control and energy balancing of the modular multilevel matrix converter. In *Power Electronics and Motion Control Conference (EPE/PEMC), 2012 15th International*, pages LS2a.3–1–LS2a.3–8, Sept 2012.
- [7] F. Kammerer, J. Kolb, and M. Braun. A novel cascaded vector control scheme for the modular multilevel matrix converter. In *IECON 2011 - 37th Annual Conference on IEEE Industrial Electronics Society*, pages 1097–1102, Nov 2011.